2018

Studying mass and mechanical property changes during the degradation of a bioadhesive with mass tracking, rheology and magnetoelastic (ME) sensors

Zhongtian Zhang
Michigan Technological University, zzhang11@mtu.edu

STUDYING MASS AND MECHANICAL PROPERTY CHANGES DURING THE DEGRADATION OF A BIOADHESIVE WITH MASS TRACKING, RHEOLOGY AND MAGNETOELASTIC (ME) SENSORS

By

Zhongtian Zhang

A THESIS

Submitted in partial fulfillment of the requirements for the degree of

MASTER OF SCIENCE

In Biomedical Engineering

MICHIGAN TECHNOLOGICAL UNIVERSITY

2018

This thesis has been approved in partial fulfillment of the requirements for the Degree of MASTER OF SCIENCE in Biomedical Engineering.

Department of Biomedical Engineering

Thesis Co-Advisor:	*Bruce P. Lee*
Thesis Co-Advisor:	*Keat Ghee Ong*
Committee Member:	*Rupak Rajachar*
Committee Member:	*Faith A. Morrison*
Department Chair:	*Sean J. Kirkpatrick*

Table of Contents

List of figures

Acknowledgements

I would like to thank Dr. Bruce P. Lee for advising my research project, training my research skills, and inspiring my continuous learning in biomedical fields. I also would like to thank Dr. Keat Ghee Ong for advising me in setting up the magnetoelastic detector, tracking the sensor responses and analyzing the results. I am sincerely grateful to Dr. Rupak Rajachar and Dr. Faith A. Morrison for being my committee members. I appreciate my colleagues Ameya Narkar and Rattapol Pinnaratip's work in proofreading my thesis. Finally, I would like to express my most sincere gratitude to my families, who always encourage and support my career in academic fields.

Abstract

In this research, the degradable polymer 4-arm poly (ethylene glycol)-glutaric acid-dopamine (PEG-GA-DM_4) was synthesized. The degradation behavior of crosslinked PEG-GA-DM_4 bioadhesive was studied with mass tracking, oscillatory rheology, and magnetoelastic (ME) sensors. Changes in mechanical properties were correlated with both dry mass and wet mass changes during the degradation. The results indicate that the loss of mechanical property in the bioadhesive can take place without losing the dry mass. The mass loss profile cannot describe the degradation behavior completely. In addition to studying the degradation of PEG-GA-DM_4, this research also confirms the application of ME sensors as a means to study the mechanical and degradation behavior of bioadhesive.

1 Introduction

Bioadhesives are materials designed to adhere to biological surfaces [1]. Some bioadhesives attach to surfaces by forming covalent [2] and ionic bonds [1], while interactions such as hydrogen bonding and van der Waals interactions can also contribute to the adhesion [1]. Besides chemical interactions, physical effects (e.g., wetting phenomenon) and mechanical effects (e.g., interpenetration) also promote adhesion to the surface [3].

Tissue adhesive is one of the applications for bioadhesive. It provides effective bleeding control and wound closure to the damaged body tissues [4]. Tissue adhesive materials vary in the market currently. FDA-approved material for tissue adhesive includes fibrin glue [5], protein-based material [6], poly (ethylene glycol) (PEG) [7] and cyanoacrylates [8]. Current tissue adhesives adhere to the tissue surfaces due to the covalent interactions. Compared to sutures, tissue adhesives have better hemostasis and wound treatment [4]. Tissue adhesive can repair the wounds caused by traumatic laceration [9]. Tissue adhesives can be designed to be degradable so that the adhesive will be removed after wound healing [10, 11]. However, the degradation may cause material failure issues at the application site due to the loss of mechanical strength in the material [12]. Such issues can cause chronic inflammation in wounds, which delays wound healing. Thus, a reliable tissue adhesive should maintain enough mechanical strength during its degradation before the wound heals completely.

Studying the mass and mechanical property changes during degradation helps researchers to have a better understanding of the bioadhesive's performance. Current

methods in studying these changes include mass tracking, oscillatory rheology, and magnetoelastic (ME) sensors. However, such studies were usually carried separately. There is a need to study both mass and mechanical property changes simultaneously because the mass loss in a material can result in mechanical property changes as well.

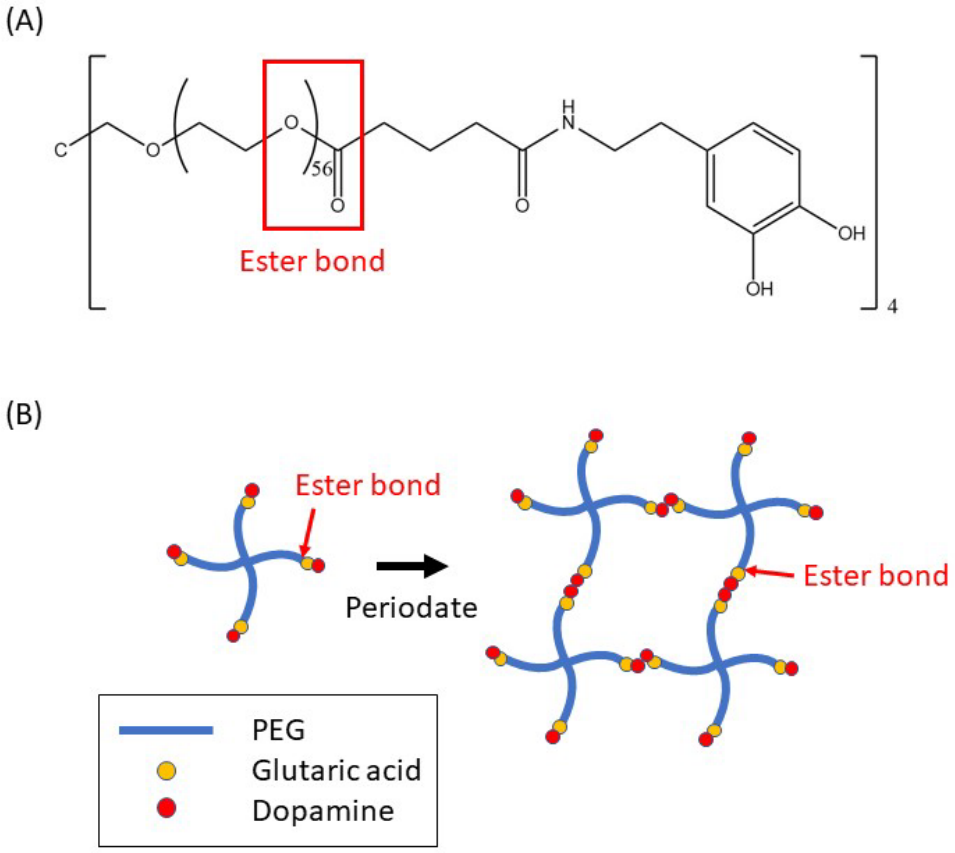

Figure 1. (A) Chemical structure of PEG-GA-DM4. (B) PEG-GA-DM4 crosslink into a network structure under the effect of periodate.

4-arm Poly (ethylene glycol)-glutaric acid-dopamine (PEG-GA-DM4) is a synthetic degradable polymer (**Figure 1A**). Poly (ethylene glycol) (PEG) is an FDA-approved biocompatible backbone material for polymers. Glutaric acid connects PEG with dopamine and contributes to the degradability of the polymer with hydrolyzable

ester bonds. Dopamine is a mussel-inspired molecule found in mussel foot proteins. It contains a catechol group, which can promote wet adhesion to both inorganic and organic surfaces through either reversible or covalent bonds. It is biocompatible, and it has been modified into many commercial PEG-based sealants [2, 13, 14]. Dopamine can be oxidized into dopamine quinone with periodate anion [15]. Dopamine quinone can further chemically crosslink and polymerize into a polymer [16]. PEG-GA-DM_4 polymers can crosslink to each other at the terminals with periodate anion due to the crosslinking of dopamine (**Figure 1B**) [16, 17]. The crosslinked polymer can form a hydrogel adhesive which adheres to the tissue due to the covalent interactions between the dopamine and the functional groups on the tissue surface. [18]

ME sensor is a novel method for tracking various parameters in situ [19]. The material of an ME sensor includes domains which can align in the same direction when a magnetic field is applied [20]. The changes in the alignment of the domains cause shape changes to the sensor. When time-varying magnetic flux is applied, the shape of the sensor changes back and forth, and the sensor exhibits longitudinal vibrations [21]. The resonance frequency and amplitude of the vibrations can be picked up with a sensing coil [19]. The resonance spectrum of the sensor is obtained by subtracting the measured sensor response to a background spectrum. When a coating exists on the sensor, changes in sensor vibrations can be utilized in detecting the mass and elasticity of the coating [21].

In this research, PEG-GA-DM_4 was synthesized and crosslinked into adhesives. Mass tracking, oscillatory rheology, and ME sensors were applied to correlate the changes in mass and mechanical properties during the bulk degradation of the adhesive.

2 Experiments

2.1 Materials

4-arm poly (ethylene glycol) 10K (PEG-10K) was purchased from JenKem Tech in China. Glutaric anhydride, N,N-Dimethylformamide (DMF), pyridine (ACS reagent, >99.0%), triethylamine, deuterium oxide (99.9 atom % D), sodium periodate ($NaIO_4$) (ACS reagent>99.8%) and Tris hydrochloride were purchased from Sigma-Aldrich in Missouri. Dopamine hydrochloride (Dopamine HCl) was purchased from ACROS Organics in New Jersey. 1-Hydroxybenzotriazole hydrate (HOBt) and O-(Benzotriazol-1-yl)-N,N,N',N'-tetramethyluronium hexafluorophosphate (HBTU) were purchased from CHEM-IMPEX in Illinois. Chloroform and phosphate buffer saline (PBS) were purchased from Fisher Scientific in Pennsylvania. Metglas 2826MB ($Fe_{40}Ni_{38}Mo_4B_{18}$) ribbon was purchased from Metglas in South Carolina. Parylene C was purchased from Specialty Coating Systems in Indiana.

2.2 Synthesizing PEG-GA-DM_4

The synthesis of PEG-GA-DM_4 followed a previously published protocol with some modifications [16, 17]. In the first step, 1 mmol of PEG-10K and 20 mmol glutaric anhydride were dissolved in 40 ml chloroform with stirring and gentle heating (55 ˚C) under nitrogen gas. When the mixture was fully-dissolved in the flask, 1.6 ml pyridine was added. The set was refluxed with nitrogen purging at 55 ˚C for overnight. The mixture was rotary-evaporated for 30 minutes to remove the chloroform and dried in a vacuum for 2 days. Dialysis of the mixture took place in deionized (DI) water in a step increasing fashion (5 minutes, 10 minutes, 15 minutes, 30 minutes, 1 hour, 6 hours, 12

hours, and 24 hours), the intermediate poly (ethylene glycol)-glutaric acid (PEG-GA_4) was dried and stored in the freezer. Glutaric acids were attached to the terminals of the PEG due to the ring-opening reaction of the cyclic glutaric anhydride.

In the next step, 0.25 mmol synthesized PEG-GA_4 was dissolved in 30 ml chloroform and 5 ml DMF in a flask. When PEG-GA_4 was fully dissolved, 2.36 mmol Dopamine HCl, 2 mmol HBTU, 1 mmol HOBt and 0.33 ml triethylamine were added. The mixture was stirred for 1 hour at room temperature. The mixture was rotary-evaporated, vacuum-dried and dialyzed by replicating the same procedures in the first step. The only modification made to the dialysis was using HCl-acidified DI water (pH 3.0) instead of DI water to prevent dopamine oxidation. PEG-GA-DM_4 was dried and stored in the freezer after the dialysis. In the reactions, HBTU converted the hydroxyl group in the carboxylic acid of the PEG-GA_4 into a leaving group. Dopamine coupled with PEG-GA_4 by forming the amide bond with glutaric acid.

2.3 PEG-GA-DM_4 characterization

2.3.1 Determining coupling efficiency with Nuclear Magnetic Resonance (NMR) spectroscopy

H-1 NMR spectroscopy (Varian 400MHz, Agilent, CA) was utilized to determine the coupling efficiency between PEG and dopamine. PEG-GA-DM_4 was dissolved in deuterium oxide solvent to make the sample. The sample concentration was 50 mg/ml. The coupling efficiency was determined by averaging the ratios between the experimental results and the theoretical values of the peaks.

2.3.2 Verification of coupling efficiency with Ultraviolet-visible (UV-vis) spectroscopy

UV-vis spectroscopy (LAMBDA35, PerkinElmer, MA) was utilized to verify the coupling between PEG and dopamine molecules [22]. A standard curve of Dopamine HCl was plotted. PEG-GA-DM_4 was dissolved in DI water, and samples (n = 5) were prepared. The concentration and absorbance of the samples were recorded. The experimental concentration of dopamine is determined by the absorbance results with Beer-Lambert law. The theoretical dopamine concentration is four times the concentration of PEG-GA-DM_4 because each PEG molecule should couple with four dopamine molecules. The ratios between the experimental and theoretical dopamine concentrations were calculated as coupling efficiency.

2.3.3 Hydrogel curing test

The gelation behavior of the polymer in forming the crosslinked hydrogel is essential for the subsequent spin-coating process [23]. Thus, the curing of PEG-GA-DM_4 needs to be studied. In a vial, 300 mg PEG-GA-DM_4 was dissolved in 1 ml 2X PBS solution to create a 300 mg/ml solution A. In another vial, 22 mg $NaIO_4$ was dissolved in 1 ml DI water to create a 0.1 M solution B. In order to initiate the gelation, 20 µl of solution B was mixed with the same amount of solution A in a glass vial. Three trials were performed, and the curing time for all the three trials was recorded. The concentration of the crosslinked hydrogel was 150 mg/ml, and the $NaIO_4$ to dopamine molar ratio was 1.

2.4 Tracking mass and mechanical properties changes during degradation

2.4.1 Preparing hydrogel discs

The hydrogel prepared in the curing test was formed into a hydrogel sheet in a custom mold made by placing a silicone sheet between two pieces of paralleled glass. The hydrogel was fully cured into a 1.5 mm-thick sheet after 24 hours. A 10 mm-diameter hole puncher was used to cut out hydrogel discs from the hydrogel sheet. The discs were 10 mm in diameter and 1.5 mm in height.

2.4.2 Tracking mechanical properties changes with rheometry

2.4.2.1 Oscillatory rheometry

Samples (n = 7) were prepared for the experiment. In each sample, hydrogel discs (n = 3) were submerged in 10 ml pH 7.4 PBS buffer in a 20 ml glass vial to degrade. All the samples were incubated at 37 ˚C. The PBS buffer in all the samples were replaced every week to maintain the pH value at 7.4. A 5 ml pipette was used to gently replace the solution in the vial with fresh the PBS buffer. A sample was taken out from the incubator, and all three hydrogel discs were tested by performing amplitude sweeps (0.01-500 strain, ν = 0.1 Hz) on them with the rheometer (HR-2, TA Instruments, DE) once a week. The discs were tested using 20 mm parallel plates. The gap distance was set at 85% of the measured thickness of each hydrogel disc. The thickness of the hydrogel discs was measured with a digital vernier caliper before the test. The storage modulus (G') and loss modulus (G") of each hydrogel disc were measured with rheometry.

2.4.2.2 Processing Loss Factor (tanδ) with storage and loss modulus results

The loss factor (tanδ) is defined as the ratio between G" and G', which gives the proportion of the dissipated energy to the stored energy [24]. The tanδ value of the hydrogels during degradation was calculated based on the rheometry results with the following equation [24]:

$$tan\delta = \frac{G"}{G'} \qquad \text{(equation 1)}$$

In this experiment, G' refers to the storage modulus at 0.1 strain in the linear elastic region, and G" is the loss modulus at the same strain.

2.4.3 Tracking mass changes

2.4.3.1 Dry mass and wet mass determination

Every time after the oscillatory rheometry test, the tested hydrogel discs were collected and dried in a vacuum for at least two days. Dry mass of each hydrogel disc was determined with the analytical balance.

Every time before the oscillatory rheometry test, the wet mass of each pending hydrogel disc was determined. The excess water on the surfaces of the hydrogel discs was removed with the Kimwipes®. The wet mass of the discs was measured with the analytical balance.

2.4.3.2 Calculate M_c and v_e with mass data

Average molecular weight between crosslinks (M_c) of the hydrogel discs was calculated based on the dry mass and wet mass data. The polymer volume fraction in the swollen hydrogel (v_{2m}) is determined by the following equation [25]:

$$v_{2m} = \frac{1}{\rho_p[(M_s/M_d) - 1] + 1} \qquad \text{(equation 2)}$$

where M_s and M_d are the mass of the hydrogels in the wetted and dried state, and ρ_p is the density of PEG (1.123 g/cm^3) [26]. The relationship between v_{2m} and M_c is demonstrated in the following Flory-Rehner equation [27]:

$$\begin{aligned} &-[\ln(1 - v_{2m}) + v_{2m} + \chi_1 {v_{2m}}^2] \\ &= (V_1/\bar{v}M_c)(1 - 2M_c/M)\left({v_{2m}}^{1/3} \right. \\ &\qquad \left. - v_{2m}/2\right) \end{aligned} \qquad \text{(equation 3)}$$

where M is the starting molecular weight of PEG-GA-DM$_4$ (10992 Da, calculated based on the chemical structure), V_1 is the molar volume of water (18.1 mol/cm^3), $\bar{v}$ is the specific volume of the polymer, and χ_1 is the polymer-solvent interaction parameter for PEG and water (0.462) [28]. The effective crosslinking density (v_e) can be calculated with M_c by applying the following equation [29]:

$$v_e = \frac{\rho}{M_c} \qquad \text{(equation 4)}$$

where ρ is the density of PEG-GA-DM$_4$. Since the density of PEG-GA-DM$_4$ is close to the density of PEG, ρ=1.123 g/cm^3 is applied [26].

2.4.3.3 Calculate G with v_e

Shear modulus (G) was calculated with v_e by applying the following equation [30]:

$$G = \left(1 - \frac{2}{f_{\text{eff}}}\right) v_e RT v_{2m} \qquad \text{(equation 5)}$$

Where f_{eff} is the effective crosslink density, v_e is the effective crosslinking density, R is gas constant, T is the temperature in kelvin, and v_{2m} is the polymer volume fraction. The f_{eff} is 4 in the calculation because each crosslink point consists of up to four PEG arms.

2.5 Tracking hydrogel degradation with ME sensors

2.5.1 Preparation of hydrogel coated ME sensors

2.5.1.1 Coating hydrogels on ME sensors

2.5.1.1.1 Pretreating bare sensors with Parylene C

Corrosion will take place during the degradation experiment because the ME sensors are made of Ferro-based materials. Parylene C was deposited to fully cover the surface of the ME sensors, which prevents the corrosion in aqueous environments [31, 32]. The deposition was carried out in a deposition system (PDS 2010 Labcoter® 2, Specialty Coating Systems, Inc., IN). The Metglas 2826MB ribbon was mechanically sheared into 12.7 mm × 5 mm × 30 μm strips for sensor usage. The deposition used 7.25 g Parylene C to achieve 10 μm-thick coatings on the ME sensors by following the

published protocol [33]. The vacuum deposition process took 4 hours. After the Parylene C deposition, the ME sensors were rinsed with ethanol and stored in a vacuum.

2.5.1.1.2 Treating Parylene C-coated sensors with polydopamine

The Parylene C-coated ME sensors were further treated with polydopamine before spin-coating. Dopamine quinone forms 5,6-dihydroxyindole after nucleophilic reaction [34]. The 5,6-dihydroxyindole can form polydopamine via covalent oxidative polymerization or physical self-assembly (e.g., π-stacking) [34]. Polydopamine adheres to Parylene C due to the π-stacking between the aromatic structures in both compounds. Depositing polydopamine on the coated ME sensor surface helps in enhancing the attachment of the adhesive to the sensor as the catechol groups in the adhesive can directly form covalent bonds with polydopamine [18, 35]. The promotion solution was created by dissolving 100 mg Dopamine HCl in 10 ml 10 mM Tris-HCl buffer. Each side of the ME sensor was exposed in the promotion solution for 30 minutes. After the polydopamine deposition, the ME sensors were dried and stored in a vacuum.

2.5.1.1.3 Spin-coating process

Spin-coating was applied to create thin homogeneous PEG-GA-DM_4 layers on the ME sensors [25, 32]. The spin-coating process was carried out on a spin coater (WS-650-23B Spin Coater, Laurell Technologies Corporation, PA). Before spin-coating, a pretreated ME sensor was fixed at the center of a glass slide. The glass slide was held in the center of the spin-coater by vacuum. Solutions A and B were prepared in the same way that has been demonstrated in the curing test section. In order to initiate the spin-

coating, 12 µl ethanol was delivered on the ME sensor to cover the sensor surface adequately. 6 µl of solution A and 6 µl of solution B were firstly mixed in a glass vial and then immediately transferred to the surface of the ME sensor. The ME sensor was spun at 1500 RPM for 4 minutes. After the spin-coating process, the coated sensors were immersed in DI water for 24 hours to remove the salts, and after that, they were dried and stored in a vacuum.

2.5.1.2 Characterization of hydrogel-coated ME sensors

2.5.1.2.1 Determining the dry mass of coated hydrogels

The dry mass of bare sensors was determined with a scientific scale before the Parylene C-coating process. The dry mass of the hydrogel-coated sensors was determined after spin-coating. The dry mass of the coated hydrogels was obtained by calculating the dry mass changes between the coated and uncoated sensors.

2.5.1.2.2 Determining the existence of PEG-GA-DM_4 on sensors with Fourier-transform infrared (FTIR) spectroscopy

FTIR spectroscopy (Perkin Elmer Spectrum One, MA) was utilized to verify the existence of PEG-GA-DM_4 hydrogels on the sensors. Both sensors before and after spin-coating were tested.

2.5.1.2.3 Morphology of the sensor under Field emission scanning electron microscope (FESEM)

The morphology of the hydrogel-coated ME sensor was studied under FESEM (Hitachi S-4700, Hitachi High Technologies America, Inc., IL). To prepare the sample

under FESEM, a coated ME sensor was cut in half and coated with platinum plasma. The cross-section view of the sensor was examined under the microscope.

2.5.2 Tracking hydrogel degradation in situ

The resonance of hydrogel-coated ME sensor strips (n = 7) were tracked by using a custom ME resonant sensor detector [36]. The detector swept the frequencies from 150 kHz to 170 kHz with 2000 mV DC offset (resolution = 20 Hz) and gave resonance amplitude results associated with the frequencies as the feedback. The amplitude was normalized by the counts that a sensor vibrated beyond a preset threshold in a fixed time span. Each sensor was submerged in pH 7.4 PBS buffer in a 2 ml glass vial individually to initiate the degradation. All the seven vials were incubated at 37 ˚C throughout the degradation. Every two days, each vial was inserted into the coil of the detector, and three frequency sweeps were run under the custom MATLAB codes. The resonance frequency and amplitude of the sensors were recorded. The tracking of the degradation lasted for 6 weeks.

2.6 Statistical analysis

Statistical analysis was performed using SigmaPlot® software (version: 12.0). One-way analysis of variance (ANOVA) was performed for comparing means between multiple groups using a p-value of 0.05.

3 Results

3.1 Nuclear Magnetic Resonance (NMR) spectroscopy

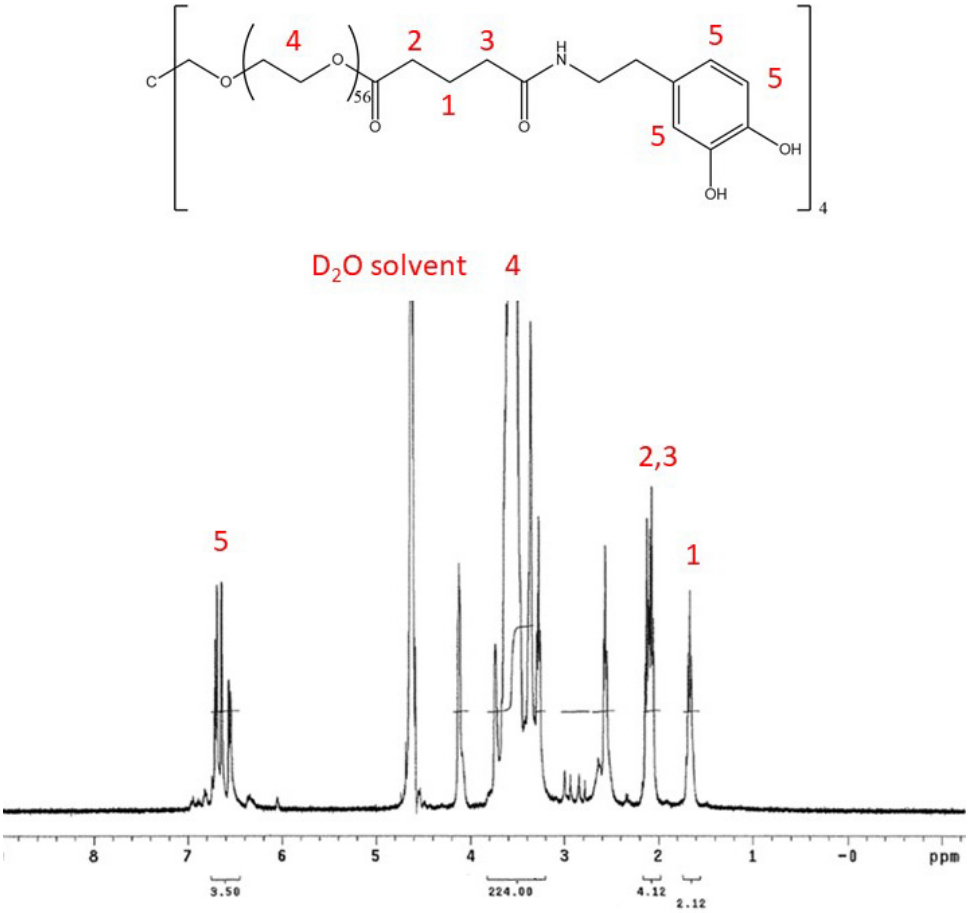

Figure 2. H-1 NMR spectrum of synthesized PEG-GA-DM4.

The H-1 NMR spectroscopy (**Figure 2**) indicated a 108% coupling between the PEG and dopamine molecules. In this case, all the branches of the PEG molecules were attached with dopamine. The coupling efficiency is greater than 100%, which indicates that there was excess dopamine in the synthesized polymers. ^{1}H NMR (400 MHz, D_2O) δ 3.75-3.37 (m, PEG), 2.17 (t, 2H, -C(=O)-CH_2-CH_2-CH_2-C(=O)-), 2.12 (t, 2H, -C(=O)-CH_2-CH_2-CH_2-C(=O)-), 1.65 (t, 2H, -C(=O)-CH_2-CH_2-CH_2-C(=O)-).

3.2 Ultraviolet-visible (UV-vis) spectroscopy

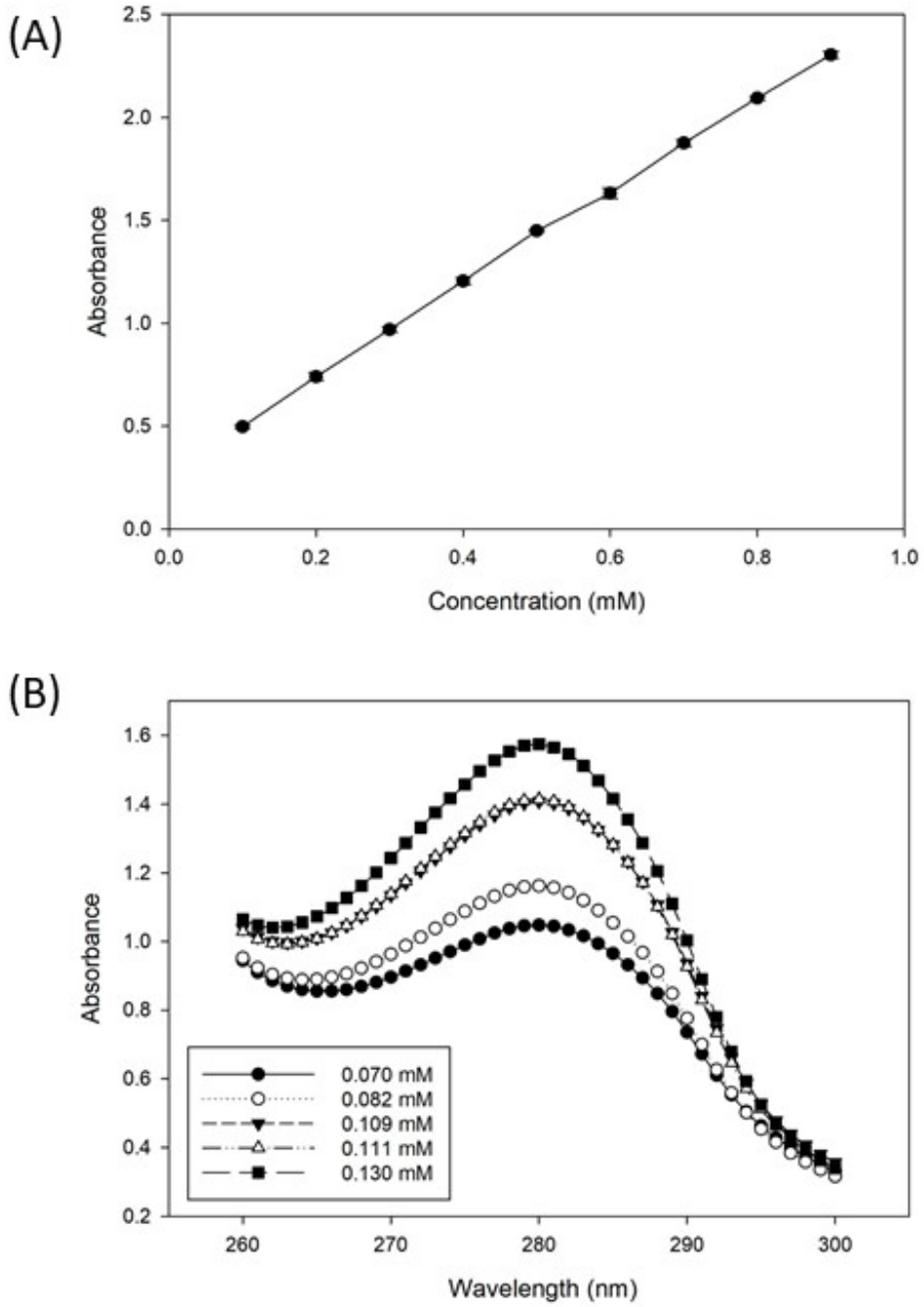

Figure 3. (A) Standard curve for dopamine at 280 nm (n = 3). (B) UV-vis spectra of tested PEG-GA-DM_4 samples (n = 5) with different concentrations (0.070 mM, 0.082 mM, 0.109 mM, 0.111 mM and 0.130 mM).

Figure 3A is a standard curve which shows a linear relationship between absorbance and dopamine concentration. The dopamine concentration in a sample can be calculated with the measured absorbance. The standard deviation is not obvious in the figure because the value was very small. **Figure 3B** is the UV-vis spectra of tested PEG-GA-DM_4 samples (n = 5) with different concentrations (0.070 mM, 0.082 mM, 0.109 mM, 0.111 mM and 0.130 mM). With the results shown in **Figure 3**, the coupling efficiency was determined as 112%. The coupling efficiency was greater than 100% because of the light scattering of the dopamine in the standard curve samples. Scattering takes place when the molecules are smaller than the wavelength of the UV light. The absorbance can be reduced compared to the theoretical value. The light scattering did not take place on the PEG-GA-DM_4 samples because the molecules were large. Compared with the NMR results, the 4-arm PEG was fully-coupled with dopamine.

3.3 Curing test

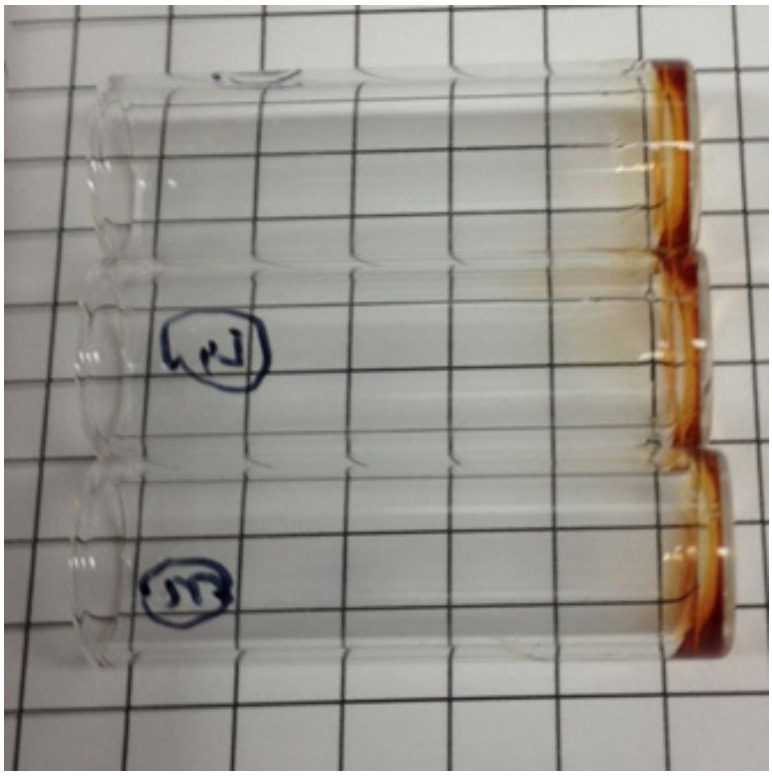

Figure 4. Cured PEG-GA-DM_4 hydrogels during curing test.

A picture of cured hydrogels is shown above (**Figure 4**). The average curing time was 30.3 ± 2.08 seconds. Hydrogels which cure around 30 seconds are optimal for forming an adhesive coating on ME sensors during spin-coating based on our tests on the spin-coater.

3.4 Oscillatory rheology

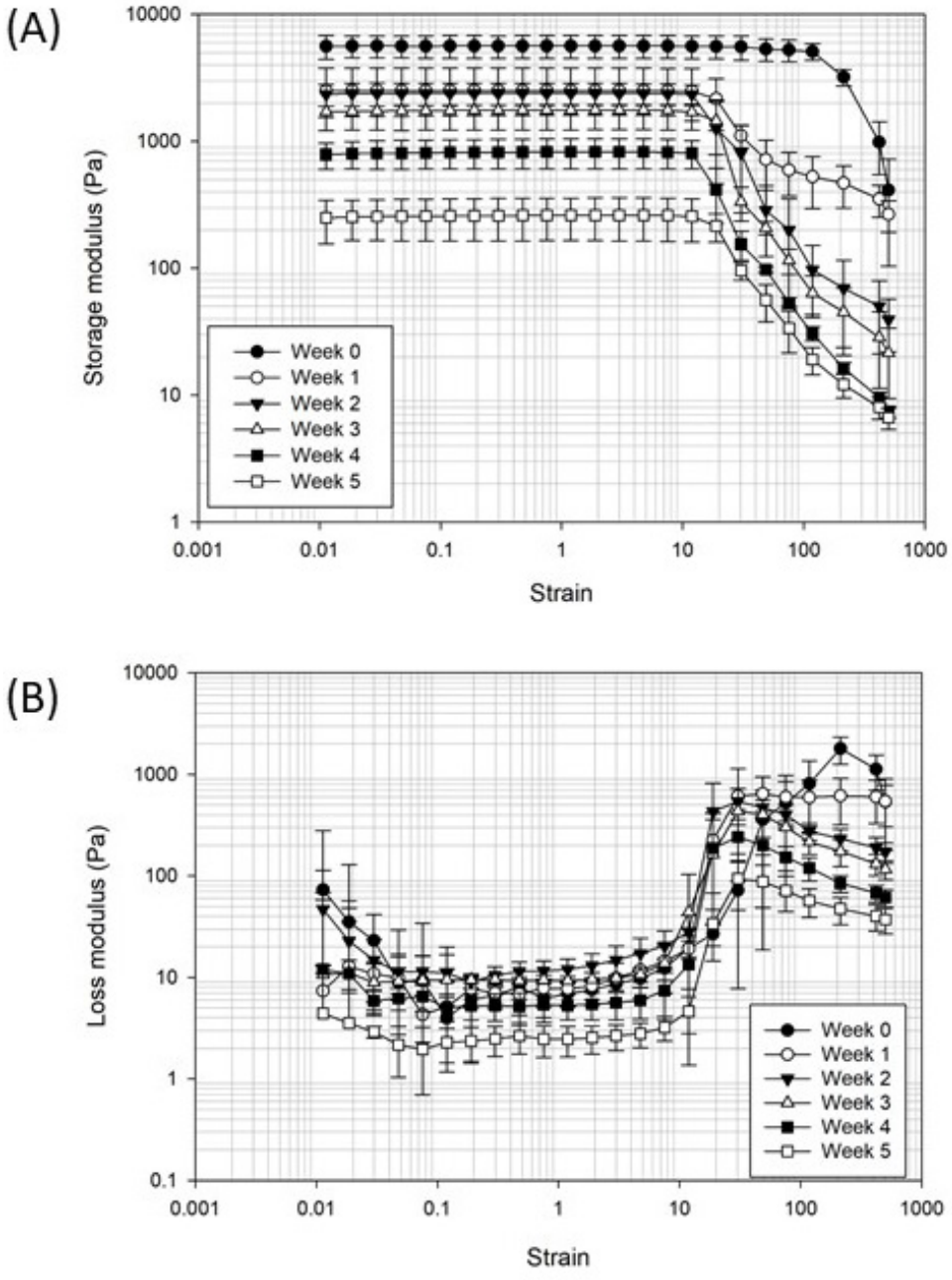

Figure 5. (A) Storage moduli of adhesives degraded over time. (B) Loss moduli of adhesives degraded over time. Adhesives were tested by performing amplitude sweeps (0.01-500 strain, v = 0.1 Hz) on them with the rheometer (HR-2, TA Instruments, DE) (*n* = 3).

G’ (**Figure 5A**) and G” (**Figure 5B**) of the adhesives during the degradation are shown above. G’ measures the stored energy, which indicates the elastic response of the material [37]. G” measures the energy dissipated as heat, which is a measure of the viscous response of a material [37]. The linear elastic regions in **Figure 5A** shows that the adhesives maintained linear elasticity when the strain increased from 0.01 to 10. The adhesives yielded as the strain continued increasing. In the linear elastic region, the G’ of the adhesives were larger than the G”, which means the adhesives are gels rather than liquids [38]. The G” of the adhesive also decreased during the degradation, but data analysis showed that the decrease in the G” was not as significant as the decrease in the G’ ($p > 0.05$).

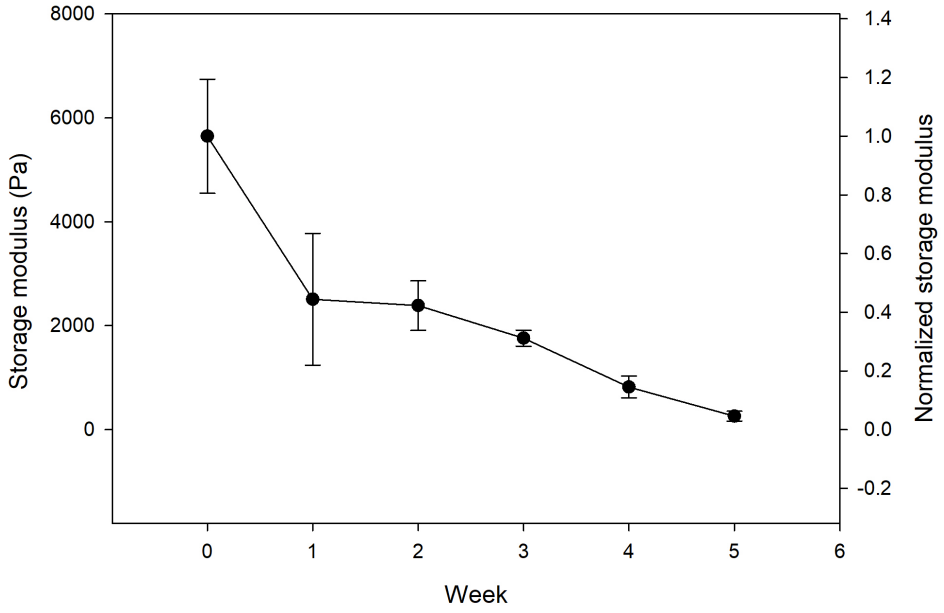

Figure 6. Storage modulus (G’) at 0.1 strain (v = 0.1 Hz) during the degradation of adhesives (*n* = 3).

G’ decreased during the degradation (**Figure 6**). The stiffness of the material reduces as G’ decreases. The adhesives become more compliant during the degradation.

G’ of the adhesive was around 6000 Pa at the beginning of the experiment. A published work prepared hydrogels from the PEG-dopamine based polymer, and reported the G’ of the hydrogel was around 6000 Pa at the beginning [17]. The G’ of the adhesive in this experiment matches the value of the published work. Data analysis suggests significant decreases appeared in the 1st, 4th and 5th week ($p < 0.05$), which indicates drastic changes to the polymer network of the adhesives may take place during these time periods.

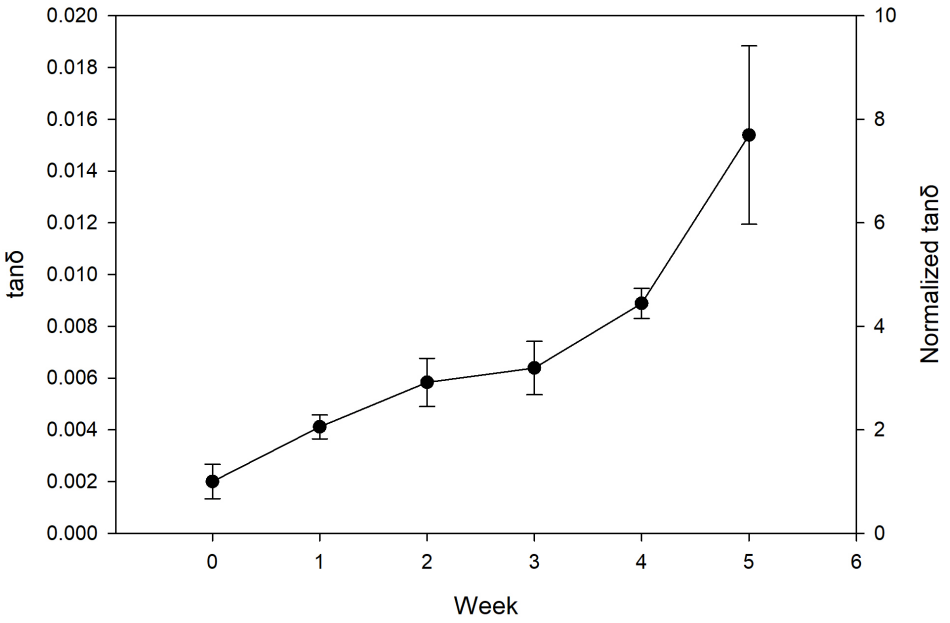

Figure 7. Loss factor (tanδ) at 0.1 strain (v = 0.1 Hz) during the degradation of adhesives (*n* = 3).

tanδ is a measure of damping in the material. During the degradation, tanδ kept increasing (**Figure 7**). Data analysis suggests a significant increase in tanδ took place every week during the degradation ($p < 0.05$). tanδ was 8 times greater than its original value by the end of the 5th week. Increased tanδ indicated that the adhesive exhibited more properties like a liquid, and it had more damping during the degradation. When the

adhesive was degrading, swelling took place. The increased water content contributed to the viscosity in the adhesive.

3.5 Dry mass and wet mass during degradation

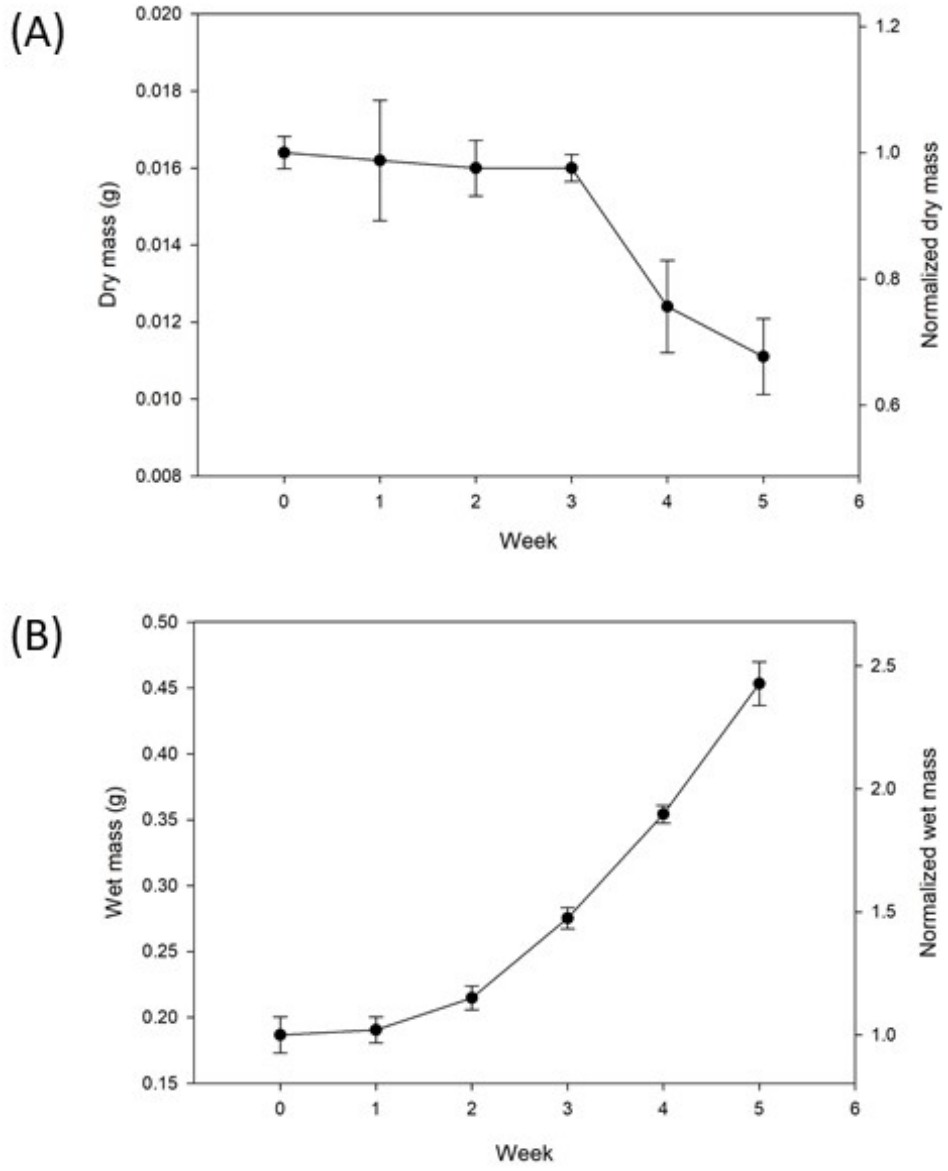

Figure 8. (A) Dry mass of the adhesives during degradation (*n* = 3). (B) Wet mass of the adhesives during degradation (*n* = 3).

Dry mass of the adhesives during degradation is shown above (**Figure 8A**). Data analysis suggests a significant 25% decrease in dry mass in the 4^{th} week ($p < 0.05$), and the dry mass loss continued. The dry mass loss in the adhesives indicates the loss of PEG polymers from the crosslinked polymer network. The hydrogels were fully degraded in the solution by the 6^{th} week. The completed degradation could also be observed. Collection of mass and rheometry data was stopped in that week.

According to **Figure 8B**, the wet mass of the hydrogel kept increasing during the degradation, which means swelling took place throughout the degradation. The wet mass of the hydrogels was 250% of the original value in the 5^{th} week. This result means more water molecules occupied the rooms in the crosslinked polymer network. Loss of the PEG in the polymer network provided vacancies for water.

3.6 Average molecular weight between crosslinks (M_c) and effective crosslinking density (v_e) during degradation

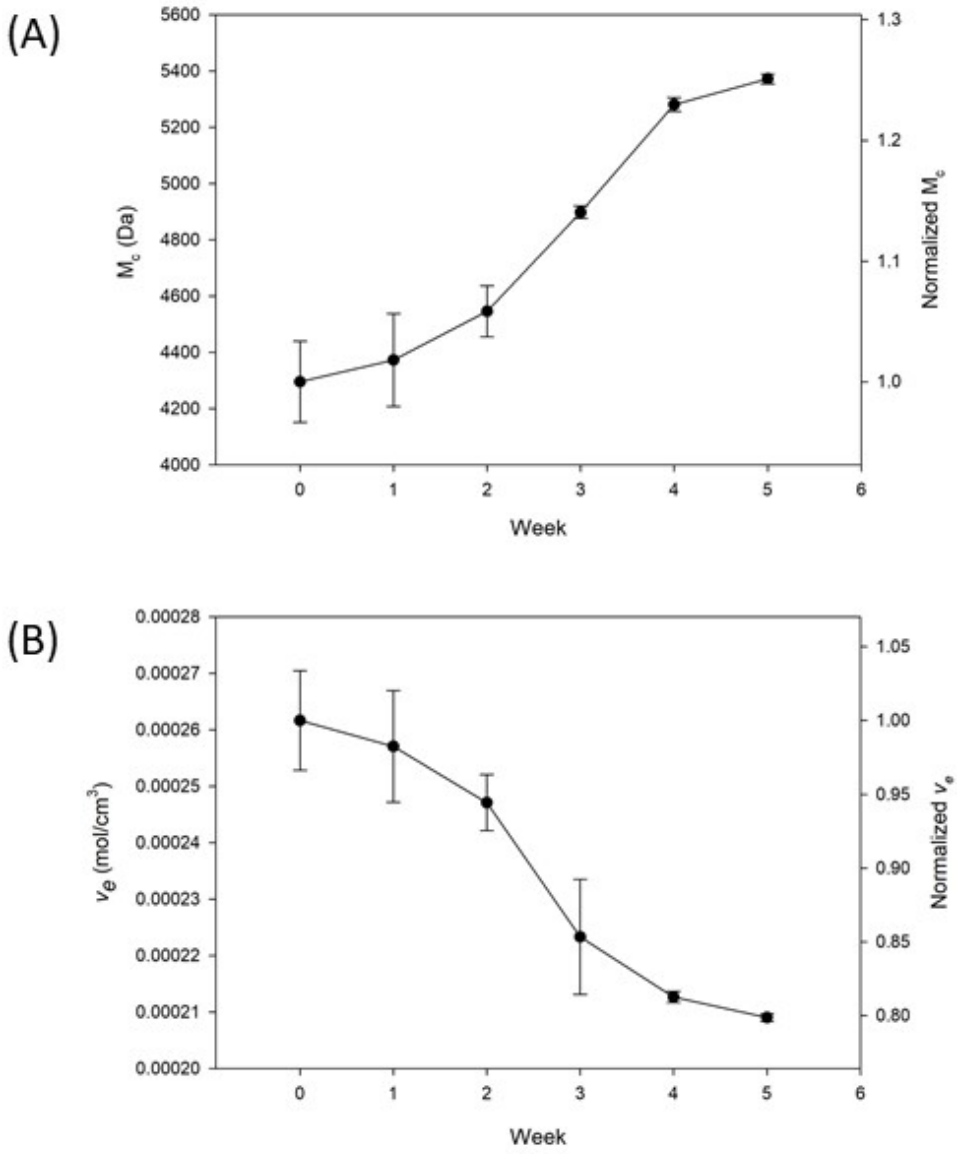

Figure 9. (A) Calculated average molecular weight between crosslinks (M_c) of the adhesives during degradation (n = 3). (B) Calculated effective crosslinking density (v_e) of the adhesives during degradation (n = 3).

M_c kept increasing during the degradation (**Figure 9A**). By the end of 5th week, M_c was 25% higher than its original value. The molecular weight of the 4-arm polymer is 10992 Da. The molecular weight of each arm is 2748 Da. The M_c of the polymer is about

4200 Da before the degradation, which is close to the molecular weight of two arms. This value means there were two polymer arms between every two crosslink points. v_e kept decreasing throughout the degradation (**Figure 9B**). It decreased to 80% of its original value in the 5th week. The decrease implies that the number of crosslink points in the polymer network reduced due to the breakdown. The loss in v_e increased the compliance of the polymer network, which reduced the stiffness of the adhesives.

3.7 Shear modulus (G) derived from v_e

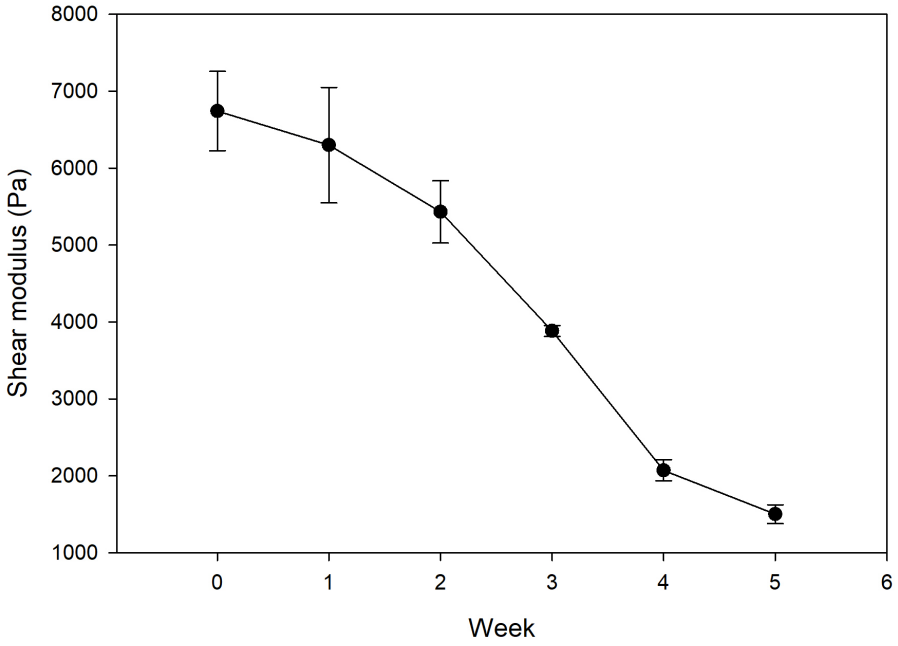

Figure 10. Shear modulus (G) derived from ve (n = 3).

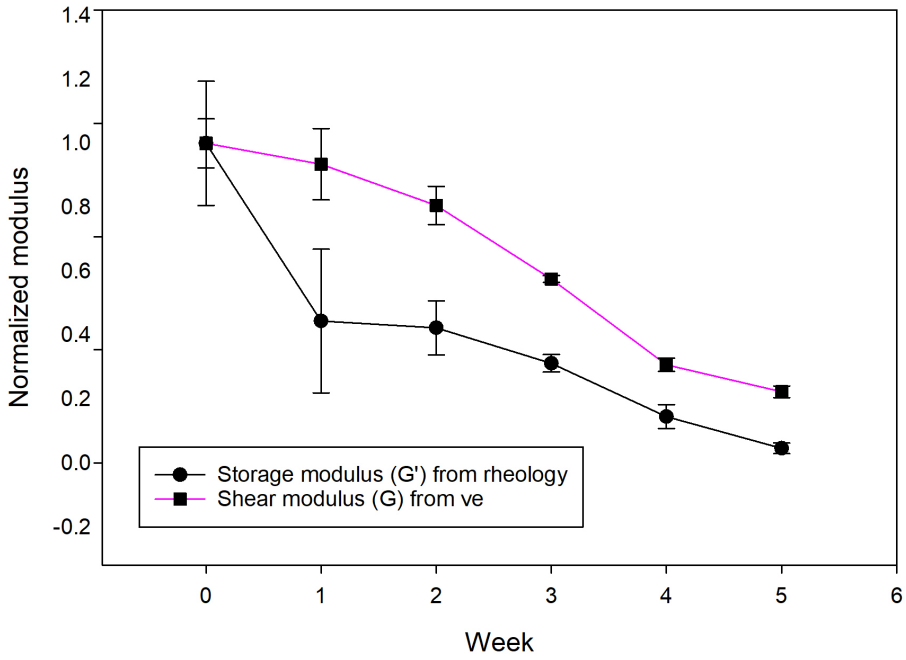

Figure 11. Storage modulus (G') and shear modulus (G) during the degradation (n = 3). G' was obtained from rheology. G was derived from effective crosslinking density (v_e).

G decreased during the degradation (**Figure 10**). G was compared with the G' from the rheology (**Figure 11**). When the degradation was initiated, the difference between G and G' was large. The breakdown of the crosslink points decreased the elasticity of the polymer network. However, the non-crosslinked PEG stayed in the polymer network because the mesh size was not large enough for the PEG to leave the network and diffuse into the water. These PEG molecules did not contribute to the elasticity of the polymer network and maintained the dry mass of the polymer. In the 4th week, the mesh size of the polymer network become large enough for the PEG to diffuse into the water, which resulted in the dry mass loss of the polymer. The dry mass loss lowered the G derived from the mass data. The difference between the G and G' become

small. The G become more accurate in estimating the elasticity when those non-crosslinked PEG molecules left the polymer network.

3.8 Fourier-transform infrared (FTIR) spectroscopy

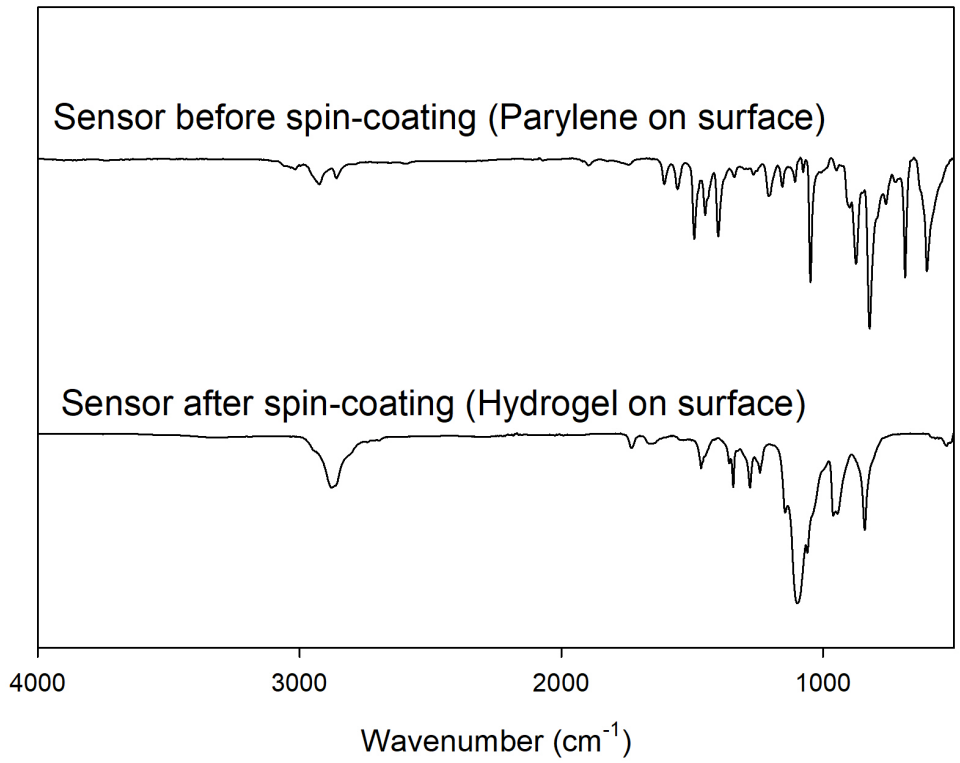

Figure 12. Fourier-transform infrared (FTIR) spectroscopy spectra of sensors with and without the hydrogel coating.

According to the FTIR spectra results (**Figure 12**), ME sensors after spin-coating exhibited PEG ether bonds (1103 cm^{-1}, -C-O-C-), carbonyl group (1727 cm^{-1}, ester linkage), and alkyl group (2878 cm^{-1}, -CH2-) peaks [17]. These peaks indicated the deposition of PEG-GA-DM_4 hydrogels on the ME sensor. ME sensors before spin-coating only exhibited aromatic structures (3000, 2924 cm^{-1}) from Parylene C [17].

3.9 Sensor morphology

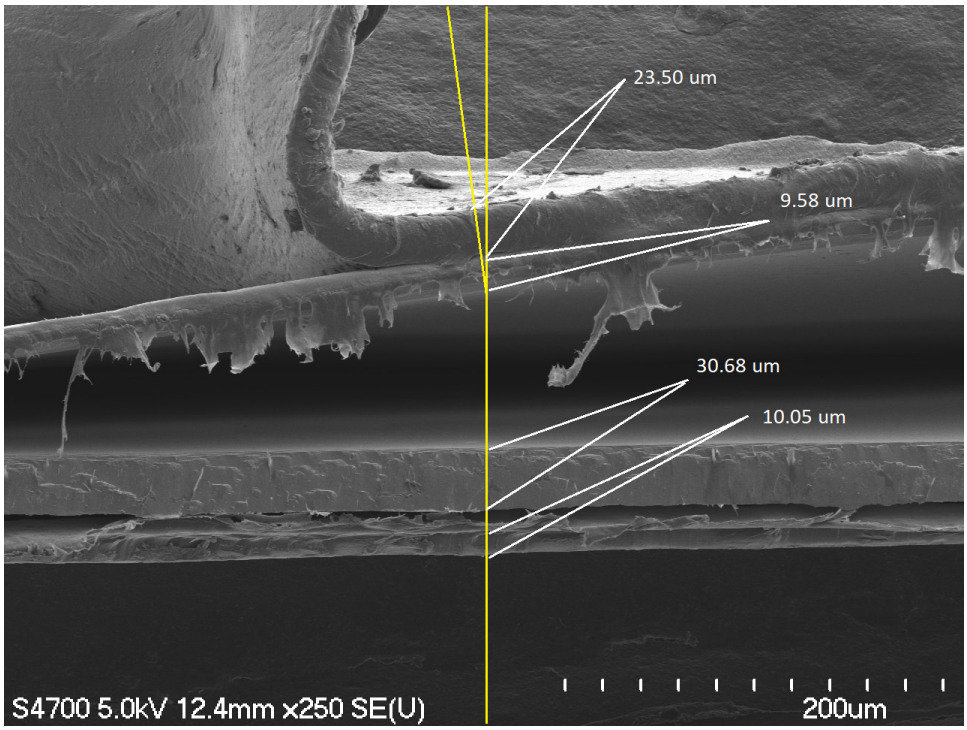

Figure 13. The cross-sectional view of a PEG-GA-DM4 hydrogel-coated ME sensor under Field emission scanning electron microscope (FESEM).

The FESEM image (**Figure 13**) showed four layers of the coated sensor: an adhesive (23.50 µm), a sensor body (30.68 µm) and two Parylene C coatings (9.58 µm, 10.05 µm). A former published paper claimed that they made hydrogel-coated ME sensors that had 23.9 ± 4.4 µm-thick adhesives, 29.8 ± 0.25 µm-thick sensor bodies and 8.6 ± 2.3 µm-thick Parylene C coatings [32]. The coating thicknesses were close to their results, and they were within our expected ranges. Delamination took place between the ME sensor layers in the FESEM image. During the degradation, the coated sensor maintained intact. No Parylene C or adhesives detached from the sensors. The observation during the experiment indicates reliable adhesions among the layers. The delamination under FESEM is due to the human artifacts when cutting the sensor.

3.10 Resonance frequency and amplitude of ME sensors

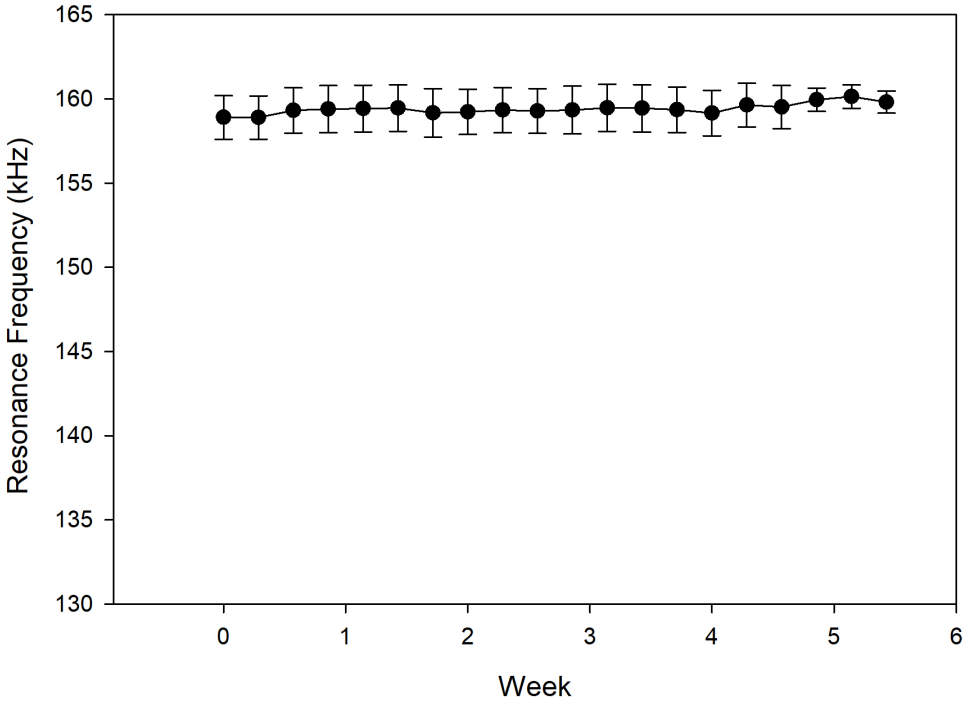

Figure 14. Resonance frequency of the hydrogel-coated ME sensors (n = 7) during degradation (resolution = 20 Hz, 2000 mV DC offset).

The sensors' average resonance frequency was around 159 kHz at the beginning and increased to about 160 kHz by the 6th week (**Figure 14**). The resonance frequency had slight changes in the first 4 weeks. The resonance frequency started to increase in the 4th week. According to the dry mass data, the hydrogel lost 30% of its dry mass by the 5th week. After applying the equation [39],

$$\Delta f = f_{load} - f_0 = -\frac{\Delta m}{2m_s} \qquad \text{(equation 5)}$$

where Δf is the change of frequency, f_{load} is the frequency with the hydrogel coating, f_0 is the frequency of the bare sensor. Δm is the dry mass changes of the coating (dry mass of the coatings = 0.0004 ± 0.0001 g), and m_s is the mass of the ME sensor

(0.0167 ± 0.0001 g). The experimental results showed a 1 kHz increase. Theoretically, the resonance frequency should have a 1.4 kHz increase by the 5th week. The noise of resonance frequency is large. Though spin-coating formed thin adhesive coatings on the sensors, the adhesives on the sensors differed. The vibration of the ME sensor is sensitive to various factors. Slight differences in the mass, elasticity, or surface morphology of the adhesive can cause frequency shifts during the vibration, which caused large noise in the frequency results. In data analysis, no significant changes in frequency took place during the degradation ($p > 0.05$). In this experiment, the resonance frequency result is not significant enough to imply the changes during the degradation of the adhesives.

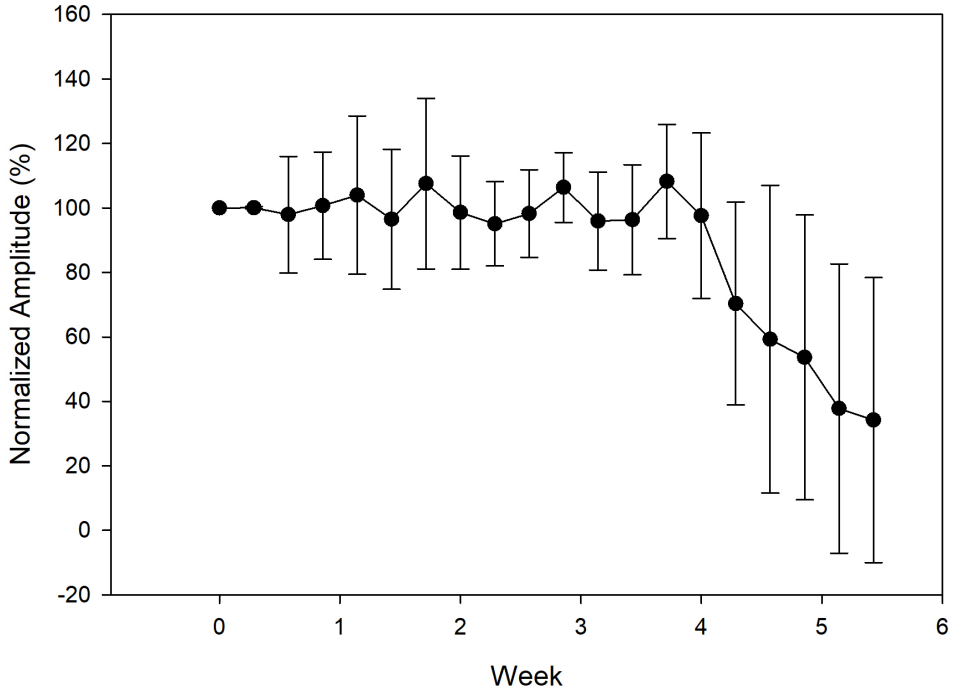

Figure 15. Resonance amplitude of the hydrogel-coated ME sensors (*n* = 7) during degradation (resolution = 20 Hz, 2000 mV DC offset).

Data analysis of the resonance amplitude results (**Figure 15**) suggests no significant changes in the first 3 weeks ($p > 0.05$). In the 4th week, significant changes in

resonance amplitude took place ($p < 0.05$). The reduction in resonance amplitude was about 60% by the 6^{th} week. The swelling increased the damping in the coated adhesive. The damping lowered down the resonance amplitude of the vibration. The degradation time of the sensors varied during the degradation. Some sensors degraded earlier than other sensors. This variation caused the large errors in the 4^{th} and 5^{th} week.

Discussions

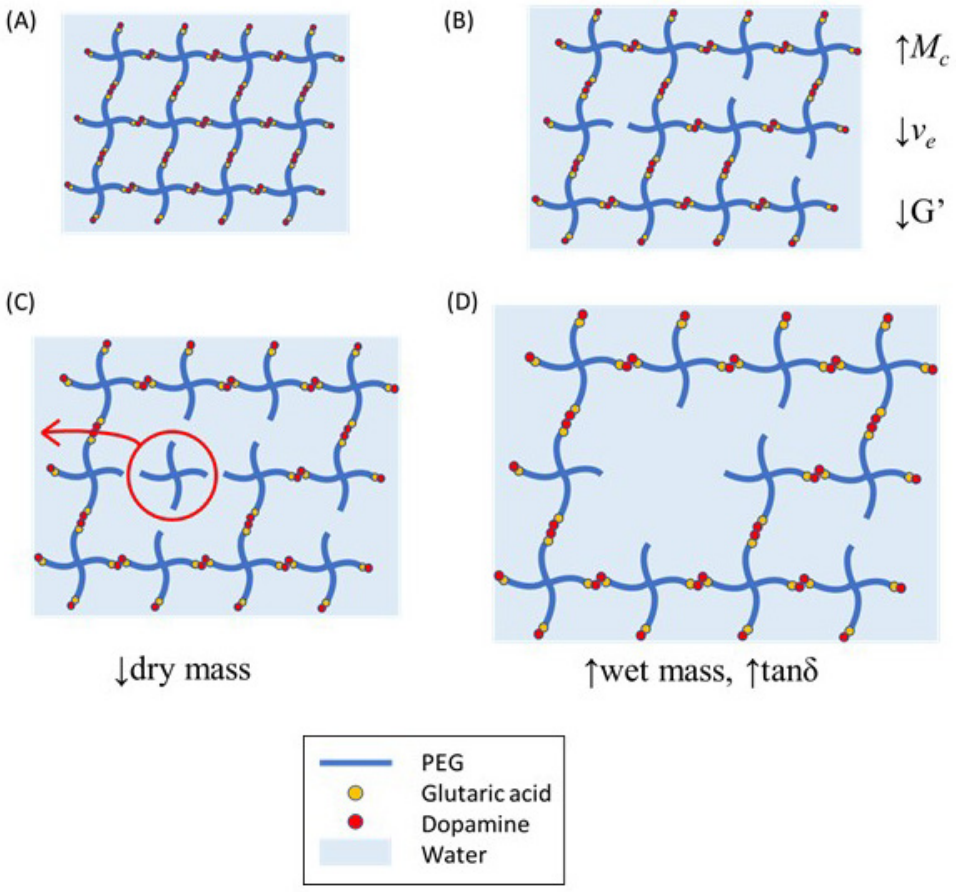

Figure 16. Proposed schematic for PEG-GA-DM4 degradation. (A) PEG-GA-DM4 forms a polymer network by crosslinking at the PEG terminals. (B) Crosslink points break down at the terminal of a PEG arm. (C) Loss of PEG in the polymer network. (D) The increased water content in the polymer network due to the loss of PEG. M_c is average molecular weight between crosslinks, v_e is effective crosslinking density, G' is storage modulus, and tanδ is loss factor.

PEG-GA-DM4 was fully crosslinked into a polymer network by forming crosslink points between two dopamine molecules with periodate (**Figure 16A**). The hydrolysis of ester bonds disconnected the dopamine from the PEG chains, which caused the breakdown of crosslink points. The reduction in crosslink points resulted in longer polymer chains between the crosslink points. The increase in M_c is a result of such

changes. Loss of crosslink points resulted in a less crosslinked polymer network (lower v_e). The density changes in the polymer network increased the compliance of the polymer. The decreased G' implies the reduced elasticity in the adhesive. The stiffness of the adhesive decreased. In the first several weeks, breakdown of crosslink points took place at the terminals of the PEG arms (**Figure 16B**). Because the mesh size of the network was not large enough for the PEG molecules to leave the network, the non-crosslinked PEG molecules stayed in the network without contributing to the elasticity of the network. No apparent dry mass changes occurred to the adhesive in this case. Starting in the 4th week, the mesh size increased during the swelling. The non-crosslinked PEG molecules left the network and diffused into water, which led to noticeable dry mass loss (**Figure 16C**). The vacancy of the detached PEG was occupied by water molecules. Increased wet mass indicates the swelling in the adhesive (**Figure 16D**), and the increased tanδ implies that the adhesive was becoming more viscous during the degradation.

The resonance amplitude results from ME sensor have correlations with the damping and the dry mass of the bioadhesive. Before the 4th week, the dry mass loss in the adhesive took place slowly because most PEG molecules were still in the polymer network. The water content between the polymers in the network was low. The mechanical impedance between the water and the polymers was small. The energy of vibration can pass through the network directly (**Figure 17A**). Thus, the damping (measured by tanδ) was not significant during this period. In this case, the ME resonance amplitude did not have significant changes. In the 4th week, a number of PEG molecules

diffused in to the water due to the loss of its crosslink points. Dry mass of the adhesive started to decrease. In the polymer network, the vacancies due to the PEG loss were occupied by the water molecules. Impedance increases when the material has components with different mechanical properties. In the adhesive, the mechanical impedance increased when more water molecules moved into the polymer network. When the energy of vibration passed through the polymer network, a part of energy bounced back due to the high impedance (**Figure 17B**). The energy was weakened after passing through the network. The loss of energy reduced the amplitude of the vibration [20]. The frequency changes fit in the expectation from the equation. However, the change in frequency is not significant. The large noise during the frequency measurement was considerable. Tracking resonance frequency is not a reliable solution in quantifying such slight mass changes of the adhesives with these sensors [21].

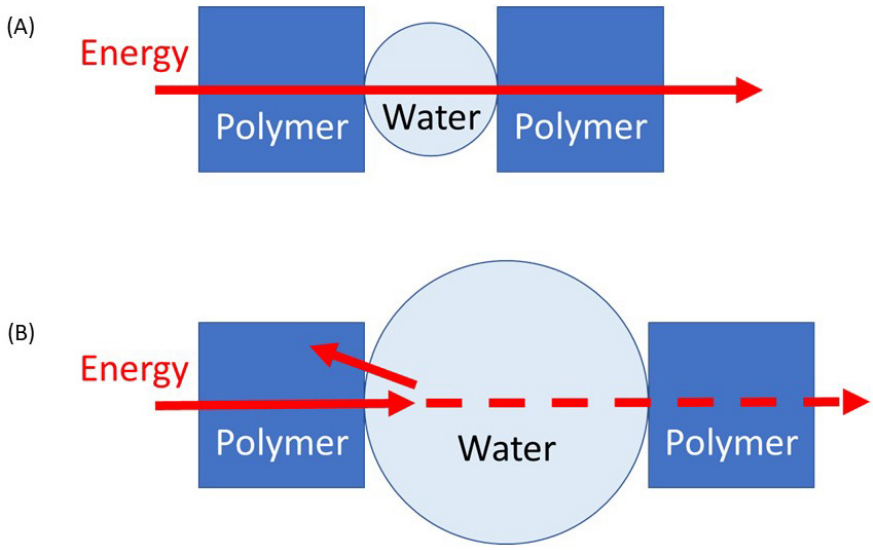

Figure 17. (A) Energy passes through the polymer network when the water content is low. (B) Loss of the energy when passing through the polymer network due to the increased water content and the mismatch of mechanical property between the polymer and the water.

The decrease in G' can be correlated with the reduction in v_e as shown in **Figure 6** and **Figure 9B**. Similarly, from **Figure 7** and **Figure 8B**, the increase in tanδ can be correlated with the changes in wet mass. Studying the dry mass and wet mass changes in the bioadhesive can interpret the mechanical property changes of the bioadhesive. In ME sensors, the reduction in resonance amplitude is due to the increased damping in the coated sensor. The increased damping can be interpreted from the increased tanδ. From **Figure 8A** and **Figure 15**, the resonance amplitude of ME sensors can be utilized in studying the mechanical property changes of the bioadhesive.

To our knowledge, we are the first to track and correlate mass changes and mechanical property changes in the degradation of branched PEG polymers with hydrolyzable ester bonds at the terminals of PEG. Branched PEG polymer is a widely studied topic in the biomedical field. Besides commercial bioadhesives, branched PEG polymers with various terminals are designed into adhesives in labs. Thermo-responsive bioadhesives with negative-thermo-swelling [40] and rapidly curing [41] features have been invented. In order to enhance the mechanical properties of the bioadhesives, silica nanoparticles [42] and alginates [43] have been added to the polymers. In tissue engineering, hydrogels made from branched PEG polymers have been applied in mimicking extracellular matrices [44]. Branched PEG polymers have been modified into carriers for drug delivery purposes as well [45, 46]. This research indicates consistent correlations between the mechanical properties and the degradation behavior of the branched terminal-modified hydrolyzable PEG-based polymers. With the methods as well as a proposed model demonstrated in this research, researchers can interpret the

mechanical property of their research material with the dry mass and wet mass results from the degradation.

4 Conclusion

A 4-arm poly (ethylene glycol)-based degradable polymer PEG-GA-DM_4 was synthesized in the lab, and the degradation behavior of the crosslinked PEG-GA-DM_4 bioadhesive was studied with mass tracking, oscillatory rheology, and magnetoelastic sensors. The results show strong correlations between both dry mass and wet mass changes, mechanical properties, and magnetoelastic (ME) resonance. The breakdown of crosslink points during the degradation detached PEG from the polymer network, which resulted in the loss of dry mass, increased wet mass, reduced storage modulus and more damping in the bioadhesive. The adhesive can lose its mechanical strength during the degradation without exhibiting the dry mass loss. Studying the mass changes during the degradation is not adequate to understand the degradation behavior completely. Moreover, the non-crosslinked PEG molecules in the polymer network can result in a larger shear modulus when estimating the elasticity of the adhesive. The elasticity can be estimated with G more accurately when the PEG molecules leaves the polymer network. The resonance amplitude of the bioadhesive-coated ME sensors can be utilized in the determination of mechanical properties during the degradation.

5 Reference List

1. Palacio, M.L. and B. Bhushan, *Bioadhesion: a review of concepts and applications.* Phil. Trans. R. Soc. A, 2012. **370**(1967): p. 2321-2347.

2. Lee, B.P., et al., *Mussel-inspired adhesives and coatings.* Annual review of materials research, 2011. **41**: p. 99-132.

3. Buonocore, M.G., *A simple method of increasing the adhesion of acrylic filling materials to enamel surfaces.* Journal of dental research, 1955. **34**(6): p. 849-853.

4. Mehdizadeh, M. and J. Yang, *Design strategies and applications of tissue bioadhesives.* Macromolecular bioscience, 2013. **13**(3): p. 271-288.

5. Wheat, J.C. and J.S. Wolf, *Advances in bioadhesives, tissue sealants, and hemostatic agents.* Urologic Clinics, 2009. **36**(2): p. 265-275.

6. Otani, Y., Y. Tabata, and Y. Ikada, *Hemostatic capability of rapidly curable glues from gelatin, poly (L-glutamic acid), and carbodiimide.* Biomaterials, 1998. **19**(22): p. 2091-2098.

7. Lee, B.P., et al., *Synthesis of 3, 4-dihydroxyphenylalanine (DOPA) containing monomers and their co-polymerization with PEG-diacrylate to form hydrogels.* Journal of Biomaterials Science, Polymer Edition, 2004. **15**(4): p. 449-464.

8. Quinn, J.V., *Tissue adhesives in clinical medicine*. Vol. 1. 2005: PMPH-USA.

9. Quinn, J., et al., *Tissue adhesive versus suture wound repair at 1 year: randomized clinical trial correlating early, 3-month, and 1-year cosmetic outcome.* Annals of emergency medicine, 1998. **32**(6): p. 645-649.

10. Bhagat, V. and M.L. Becker, *Degradable Adhesives for Surgery and Tissue Engineering.* Biomacromolecules, 2017. **18**(10): p. 3009-3039.

11. Peng, B., et al., *Scarless Wound Closure by a Mussel-Inspired Poly (amidoamine) Tissue Adhesive with Tunable Degradability.* ACS Omega, 2017. **2**(9): p. 6053-6062.

12. Donkerwolcke, M., F. Burny, and D. Muster, *Tissues and bone adhesives—historical aspects.* Biomaterials, 1998. **19**(16): p. 1461-1466.

13. Lu, Q., et al., *Adhesion of mussel foot proteins to different substrate surfaces.* Journal of The Royal Society Interface, 2013. **10**(79): p. 20120759.

14. Kord Forooshani, P. and B.P. Lee, *Recent approaches in designing bioadhesive materials inspired by mussel adhesive protein.* Journal of Polymer Science Part A: Polymer Chemistry, 2017. **55**(1): p. 9-33.

15. Liu, B., L. Burdine, and T. Kodadek, *Chemistry of periodate-mediated cross-linking of 3, 4-dihydroxylphenylalanine-containing molecules to proteins.* Journal of the American Chemical Society, 2006. **128**(47): p. 15228-15235.

16. Lee, B.P., J.L. Dalsin, and P.B. Messersmith, *Synthesis and gelation of DOPA-modified poly (ethylene glycol) hydrogels.* Biomacromolecules, 2002. **3**(5): p. 1038-1047.

17. Liu, Y., et al., *Injectable dopamine-modified poly (ethylene glycol) nanocomposite hydrogel with enhanced adhesive property and bioactivity.* ACS applied materials & interfaces, 2014. **6**(19): p. 16982-16992.

18. Liu, Y., et al., *Biomimetic Adhesives and Coatings Based on Mussel Adhesive Proteins*, in *Biological Adhesives*. 2016, Springer. p. 345-378.

19. Grimes, C.A., et al., *Wireless magnetoelastic resonance sensors: A critical review.* Sensors, 2002. **2**(7): p. 294-313.

20. Hubert, A. and R. Schäfer, *Magnetic domains: the analysis of magnetic microstructures*. 2008: Springer Science & Business Media.

21. Roy, S.C., et al., *Quantification of blood clotting kinetics II: Thromboelastograph analysis and measurement of erythrocyte sedimentation rate using magnetoelastic sensors.* Sensor Letters, 2007. **5**(2): p. 432-440.

22. Andersen, S.O., et al., *Phenoloxidase catalyzed coupling of catechols. Identification of novel coupling products.* Biochimica et Biophysica Acta (BBA)-Protein Structure and Molecular Enzymology, 1992. **1118**(2): p. 134-138.

23. Liu, Y., et al., *Marine adhesive containing nanocomposite hydrogel with enhanced materials and bioadhesive properties.* MRS Online Proceedings Library Archive, 2013. **1569**: p. 33-38.

24. Seidel, C., et al., *Influence of the cross-linking agent on the gel structure of starch derivatives.* Starch-Stärke, 2001. **53**(7): p. 305-310.

25. Cencer, M., et al., *Effect of pH on the rate of curing and bioadhesive properties of dopamine functionalized poly (ethylene glycol) hydrogels.* Biomacromolecules, 2014. **15**(8): p. 2861-2869.

26. Arlie, P.J., P. Spegt, and A. Skoulios, *Etude de la cristallisation des polymères. II. Structure lamellaire et repliement des chaines du polyoxyéthylène.* Die

Makromolekulare Chemie: Macromolecular Chemistry and Physics, 1967. **104**(1): p. 212-229.

27. Alger, M., *Polymer science dictionary*. 1996: Springer Science & Business Media.

28. Merrill, E.W., K.A. Dennison, and C. Sung, *Partitioning and diffusion of solutes in hydrogels of poly (ethylene oxide).* Biomaterials, 1993. **14**(15): p. 1117-1126.

29. Barcellos, I.O., A.T.N. Pires, and I. Katime, *Physical properties of hydrogels of poly (2-hydroxyethyl methacrylate) and copolymers with mono-methyl itaconate synthesized by bulk and solution polymerization.* Polymer international, 2000. **49**(8): p. 825-830.

30. Ding, X., et al., *Nitro-Group Functionalization of Dopamine and its Contribution to the Viscoelastic Properties of Catechol-Containing Nanocomposite Hydrogels.* Macromolecular chemistry and physics, 2015. **216**(10): p. 1109-1119.

31. Schwarz, J.A., C.I. Contescu, and K. Putyera, *Dekker encyclopedia of nanoscience and nanotechnology*. Vol. 3. 2004: CRC press.

32. Lin, M.-H., et al., *Monitoring the long-term degradation behavior of biomimetic bioadhesive using wireless magnetoelastic sensor.* IEEE Transactions on Biomedical Engineering, 2015. **62**(7): p. 1838-1842.

33. Holmes, H.R., et al., *Biodegradation and biocompatibility of mechanically active magnetoelastic materials.* Smart Materials and Structures, 2014. **23**(9): p. 095036.

34. Hong, S., et al., *Non-covalent self-assembly and covalent polymerization co-contribute to polydopamine formation.* Advanced Functional Materials, 2012. **22**(22): p. 4711-4717.

35. Shafiq, Z., et al., *Bioinspired underwater bonding and debonding on demand.* Angewandte Chemie, 2012. **124**(18): p. 4408-4411.

36. Ong, K.G., et al., *A rapid highly-sensitive endotoxin detection system.* Biosensors and Bioelectronics, 2006. **21**(12): p. 2270-2274.

37. Han, C.D. and M.S. Jhon, *Correlations of the first normal stress difference with shear stress and of the storage modulus with loss modulus for homopolymers.* Journal of Applied Polymer Science, 1986. **32**(3): p. 3809-3840.

38. Almdal, K., et al., *Towards a phenomenological definition of the term 'gel'.* Polymer gels and networks, 1993. **1**(1): p. 5-17.

39. Grimes, C., et al., *Remote query pressure measurement using magnetoelastic sensors.* Review of Scientific Instruments, 1999. **70**(12): p. 4711-4714.

40. Zhang, H., et al., *On-demand and negative-thermo-swelling tissue adhesive based on highly branched ambivalent PEG–catechol copolymers.* Journal of Materials Chemistry B, 2015. **3**(31): p. 6420-6428.

41. Sanborn, T.J., P.B. Messersmith, and A.E. Barron, *In situ crosslinking of a biomimetic peptide-PEG hydrogel via thermally triggered activation of factor XIII.* Biomaterials, 2002. **23**(13): p. 2703-2710.

42. Pinnaratip, R., et al., *Effect of incorporating clustered silica nanoparticles on the performance and biocompatibility of catechol-containing PEG-based bioadhesive.* Biomedical Materials, 2018. **13**(2): p. 025003.

43. Jeon, O., J.E. Samorezov, and E. Alsberg, *Single and dual crosslinked oxidized methacrylated alginate/PEG hydrogels for bioadhesive applications.* Acta biomaterialia, 2014. **10**(1): p. 47-55.

44. Bryant, S.J. and K.S. Anseth, *Controlling the spatial distribution of ECM components in degradable PEG hydrogels for tissue engineering cartilage.* Journal of Biomedical Materials Research Part A: An Official Journal of The Society for Biomaterials, The Japanese Society for Biomaterials, and The Australian Society for Biomaterials and the Korean Society for Biomaterials, 2003. **64**(1): p. 70-79.

45. Alconcel, S.N., A.S. Baas, and H.D. Maynard, *FDA-approved poly (ethylene glycol)–protein conjugate drugs.* Polymer Chemistry, 2011. **2**(7): p. 1442-1448.

46. Henise, J., et al., *Biodegradable tetra-PEG hydrogels as carriers for a releasable drug delivery system.* Bioconjugate chemistry, 2015. **26**(2): p. 270-278.